4n+2=6n? A Geometrical Approach to Aromaticity?

Aristides D. Zdetsis*

Molecular Engineering Laboratory, Department of Physics, University of Patras, Patras 26500 GR, Greece, and

Institute of Electronic Structure and Laser, Foundation for Research &Technology Hellas, Vassilika Vouton, P.O. Box 1385, Heraklion, Crete GR-71110, Greece

ABSTRACT

Using a simple, but powerful geometrical/topological notion of aromaticity, based on the shell model [*J. Phys. Chem. C*, **2018**, 122, 17526] and the bipartite topology, we uncover, on top of the essential equivalence of the fundamental Hückel's and Clar's rules of aromaticity, the significance of empty peripheral rings, which are shown to be linked to zigzag edge states. Such empty rings can be thought of as "inversion symmetry incompatible". Thus, elimination of these rings under the existing symmetry constrains preserves the aromaticity pattern and leads to substantial improvement of the stability and/or sublattice imbalance, resulting in larger electronic bandgaps, and lack of zigzag edge/end states. Using these ideas, we can illustrate that trigonal D_{3h}-symmetric nanographens cannot be graphene-like, because they are either armchair without Dirac points, or zigzag bonded (triangulenes) topologically frustrated with high spin states. This is also true for hexagonal heteroatomic BN or SiC structures, contrary to homoatomic silicene, germanene, etc. Existing paradigms are highly suggestive that such elimination process could occur naturally.

*zdetsis@upatras.gr

TOC Graphic

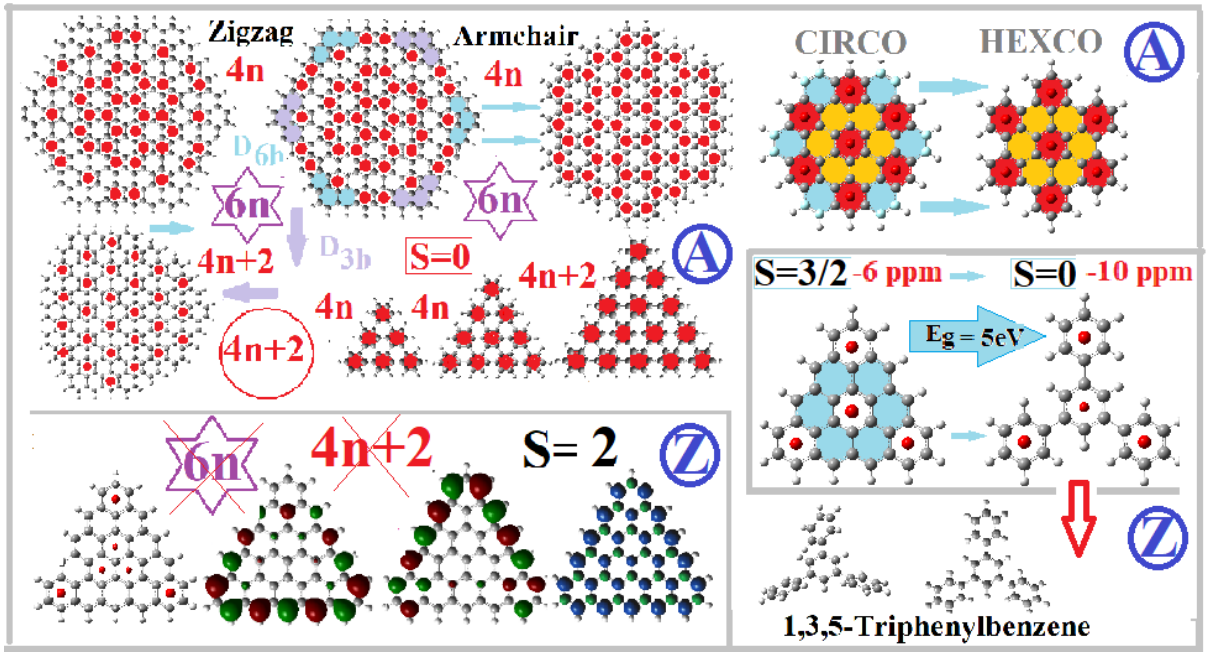
Zigzag
Armchair
4n
4n
D6h
6n
6n
4n+2
D3h
S=0
4n+2
4n
4n
4n+2
A
6n
4n+2
S= 2
Z
CIRCO
HEXCO
A
S=3/2 -6 ppm
S=0 -10 ppm
Eg = 5eV
Z
1,3,5-Triphenylbenzene

1. Introduction. The molecular approach of graphene through a well-defined sequence of growing size polycyclic aromatic hydrocarbons (PAHs) has been recently proven a very successful and insightful approach, deciphering at the molecular level all or most of the "exotic" properties of graphene.[1-3] This approach was able to pinpoint the deeper roots and origins of such properties as Dirac points, and to provide totally new information and interpretation(s).[1-3] It was revealed for example that graphene is the analogous crystalline prototypical aromatic solid in full analogy to the prototypical aromatic molecule of benzene[2]. The new emerging feature is the dominant role of aromaticity (in all of its forms, expressions and manifestations), combined with topology and symmetry, which seem to be inherently connected to aromaticity. The driving force is the molecular versus (sub)lattice symmetry competition, which can be also seen as a competition between two different chiral forms or different sublattices A and B. All these properties are interrelated in known and unknown, but mostly indirect ways, which are here revealed in a "one-to-one" correspondence. We illustrate in this work, using a "geometrical" approach to aromaticity, based on the shell model[1] and symmetry arguments stemming from the bipartite topology (or the alternant hydrocarbon nature of the underlying PAHs) that we can directly link the empty peripheral (edge) rings with the zigzag edge-bonds and the associated topological edge/end states[4]. This can lead to guided molecular engineering, in several cases analogous to the pioneering synthesis of 3-triangulene, using the tip of a scanning tunnelling microscope (STM) to physically move individual atoms[5] (and rings). Thus, the present methodology, extended to topologically frustrated structures, can help to substantially relief the sublattice imbalance, which is responsible for the violation of the well-known Kekulé bonding rules. This can be achieved based solely on the geometry and symmetry of the "aromaticity pattern", which can be generated even for

non-fully aromatic molecules, by reducing the "aromaticity threshold" (critical value of the adopted aromaticity index). However, for really aromatic molecules (not topologically frustrated) such as PAHs and nanographenes (NGRs), the same technique, as we show here, can substantially improve their electronic, aromatic, and structural properties in a fully coordinated way. The guiding principles are based on the "shell model"[1] through which we are led to "improve" or re-interpret the fundamental aromaticity rules of Hückel (4n+2) and Clar (6n), which for hexagonal PAHs in the framework of the shell model can be considered as equivalent.[1-2] Such rules reflect Kekulé's bonding rules and ideas about aromaticity and "stability". Yet, unstable (highly reactive) structures which violate Kekulé's rules, such as various triangulenes[5-7] and other "elusive" structures[8] have been recently synthesized using novel bottom up atomically precise techniques, employing suitable precursors on metallic substrates. Obviously, such structures violate Kekulé rules and, consequently, important symmetry requirements linked to aromaticity (and stability). One of the essential symmetries is inversion symmetry, which is directly connected with sublattice imbalance and topological competition between molecular and sublattice symmetry groups. Such constructive symmetry competition is responsible for the exotic properties of graphene, and graphene-based or graphene-like structures, including PAHs, NGRs, and armchair graphene nanoribbons (AGNRs).[1-3] Among the properties directly or indirectly related with such symmetry competition are Dirac points[3] and topological end/edge states.[4] Therefore, all these structures (aromatic and frustrated) can be constructively manipulated, guided by the principle of eliminating (or generating, if the opposite is desired) inert (empty) peripheral benzene rings, within the symmetry constrain(s). Such "inert" rings, within the shell model, are "compatible" with unoccupied, rather than occupied molecular orbitals, and with the next shell structure (rather than the current).

Thus, they are associated with opposite inversion (parity of HOMO/LUMO) properties, which are rather incompatible with the current, but fully compatible with the next. This is why they are fully aromatic in the next shell structure, *vide infra*. We demonstrate these ideas here by applying them to hexagonal and triagonal PAHs and NGRs as well as rectangular AGNRs. In principle such technique can be applied to other honeycomb based hexagonal or trigonal structures sharing the bipartite topology, including silicene, germanene, etc., in their buckled D_{3d} geometry, in contrast to the heteroatomic BN or SiC D_{3h} symmetric structures. This is because in the homoatomic D_{3d} structures (with center of inversion) the molecular and sublattice symmetry groups are different, whereas in the heteroatomic D_{3h} structures (with no inversion center) the molecular and sublattice groups are identical. We should recall here that the competition between the molecular and sublattice symmetry groups is the driving force for the characteristic properties of graphene (Dirac points, etc.). In the present work we apply these ideas and concepts to uncover and demonstrate basic principle(s) for guided molecular (or rather ring) engineering which allows, among others, the successful and promising transformation of zigzag structures to armchair ones with improved properties such as aromaticity, and energy gaps. The energy gaps between highest occupied and lowest unoccupied molecular orbitals, HOMO and LUMO respectively, for larger sizes represent the bandgap between valence and conduction bands. The same methodology can lead, if desired, to the formation of stable and naturally abundant molecules (or crystals) from totally unstable or elusive molecules, such as the various triangulenes. The central idea in such cases is to chemically or mechanically (e.g. with the STM tip) remove the “empty” (non-aromatic) peripheral rings, as is described below. The examples of molecular pairs such as circum-coronene (CIRCO) and hexabenzocoronene (HEXCO), or of extended 4-triangulene and 1, 3, 5-

triphenylbenzene are highly suggestive that the suggested "truncation" process could eventually be a natural process. This could be very important, intriguing, and illuminating. In what follows, the theoretical and calculational framework is reviewed and summarized in section 2. In section 3, the results and discussion for hexagonal (3.1) and triagonal (3.2) NGRs are presented, separately for armchair (3.2.1), and zigzag (3.2.2) structures, whereas D_{2h}-symmetric rectangular AGNRs are considered in section 4. Finally, the main conclusions of the present work are summarized in section 5. Additional information is included as supplementary information (SI).

2. Theoretical and Computational Framework.

2.1 Current Theoretical Approaches. The customary concepts and computational tools used for the description of PAHs and NGRs are historically based on the fundamental ideas and rules of Kekulé in conjunction with the properties of alternant (or bipartite) hydrocarbons, using either the tight-binding (TB) model, or the more sophisticated one-orbital Hubbard model (in the mean field approximation), supplemented in many cases by chemical graph theory.[9-11] The key concepts of chemical graph theory are the sublattice imbalance expressed by the number N_A-N_B (the difference in the total number of sublattice sites A and B; and the nullity η, which is defined topologically as the difference between the maximum numbers of non-adjacent vertices and edges respectively).[9-11] For the high symmetry structures examined here, PAHs and NGRs, in which at most one sublattice is topologically frustrated, η is equal to the lattice imbalance, $\eta=|N_A-N_B|$, although in other cases, where both sublattices are frustrated,[9] η could be nonzero even when$=|N_A-N_B|=0$, as in the case of Clar's goblet.[8-9] Within the tight binding (TB) approximation in which the TB Hamiltonian H_0 includes only nearest neighbor interactions, the nullity η is equal to the number of nonbonding zero-energy states. This is also true for more advance models

based on the TB description, such as the Hubbard model which includes (on-site) electron correlation (through the "Hubbard U"). In this case such non-bonding states can get spin polarized. In this case η also represents the number of singly occupied spin polarized states. The simplest one-orbital Hubbard model in the mean field approximation (see averages < > below), is described by the Hamiltonian:

$$\left\{ \begin{array}{l} H = H_0 + U\sum_i n_{i\uparrow} < n_{i\downarrow} > + < n_{i\uparrow} > n_{i\downarrow} \quad , \\ H_0 = -t\sum_{i,\mathrm{j},\sigma} c_{i\sigma}^{\dagger} c_{j\sigma} + c_{i\sigma} c_{j\sigma}^{\dagger} \end{array} \right\} \quad (1) \, ,$$

where H_0 is the usual TB Hamiltonian with t ($t \approx 2.7$ eV) the hopping integral and $c_{i\sigma}^{\dagger}, c_{i\sigma}$ the creation, annihilation operators, respectively, which create and annihilate an electron at site i with spin σ. U is the on-site Coulomb interaction, and $n_{i\uparrow} = c_{i\uparrow}^{\dagger}, c_{i\uparrow}$ and $n_{i\downarrow} = c_{i\downarrow}^{\dagger}, c_{i\downarrow}$ are the number operators at site i with spin up and spin down respectively. The mean field one orbital Hubbard model, despite the simplifying assumptions is still very much computationally demanding[9-11], and the results depend on the choice of the parameter U/t.

2.2 The Present Approach. Here we use a fully quantitative description based on series of density functional theory (DFT) calculations in a well-defined sequence of PAHs (termed the "main sequence") supplemented by simple topological arguments of symmetry and aromaticity emerging from the shell model[1] and the bipartite (alternant) topology. The main sequence of PAHs, shown in Fig. S1, was invoked to describe graphene through appropriate extrapolation of the properties and trends of the individual PAHs. Such approach has been shown[2-3] not only to be adequate for the description and modelling of the individual hexagonal PAHs, but through the comparative study of such PAHs in terms of size, it indirectly includes some key

characteristics of the many-body theory description (of the electron-electron interaction)[1-3] of graphene. In particular, some consequences of inversion symmetry frustration in the sublattice symmetry group, which is based in the bipartite topology and the notion of pseudospin (where, as usual, pseudospin up means sublattice site A, and pseudospin down is equivalent to sublattice site B) have been directly related with exotic properties of graphene. However, here we follow the reverse route from graphene to benzene and concentrate on the individual intermediate PAHs, taking into account the trends and conclusion from the molecular description of graphene.[2-3] Consequently we emphasize here general symmetry characteristics and their intimate interconnection with aromaticity, which are the key characteristics of both ends of the route: graphene and benzene. It should be mentioned at this point that we should recognize that the formalism of eqs. (1) described above, could be also considered (with obvious minor modifications) as describing the pseudospin, related with "sublattice" properties and symmetries. Therefore, Lieb's theorem[9] and other important conclusions based on it should be valid for pseudospin as well, entering (directly or indirectly) the present theoretical framework. Pseudospin or sublattice symmetry, which is a manifestation of chirality, is one important cornerstone of the present theoretical framework; the second is aromaticity (in its simplest geometrical notion). The concept of symmetry in Chemistry is not totally geometrical because seen as a mathematical point, a carbon atom with a lone pair or with an unbalanced number of (Kekulé-type) bonds, which is "topologically frustrated", like in Clar's goblet,[8-9] is not "chemically equivalent" to another carbon atom with normal balanced bonding. Likewise, carbon atoms with different environment or "chirality", belonging to different sublattices, are not (physically/chemically) equivalent. Aromaticity, on the other hand, which is an extremely important and useful property, is often considered as a very "complicated",

misunderstood, or redundant concept, largely controversial.[12-14] Most of the confusion arises not only from the fact that aromaticity is not a measurable quantity (which, however is common to many key properties in Chemistry), but mostly, according to Hoffman,[12] from various, sometime obscure, extensions of the original concept of aromaticity (which basically means "like benzene"), and a rather large number of aromaticity types, indices and criteria. In several cases such plethora of aromaticity indices could be conflicting with each other, although each one of these could serve a specific purpose.[13-14] Nevertheless, these subtle points which cannot undermine the great importance and usefulness of aromaticity, have no direct implications in the present work. The simple and basic notion of aromaticity, as is adopted and applied here (requiring minimal basic knowledge, but no special or advanced aromaticity concepts and methods), is proven[1-4, 16-17] an extremely useful, simple, powerful, and insightful "everyday" tool (see computational Methods below, in section 2.3). The central concept here is the "aromaticity pattern" i.e., the spatial distribution of aromatic (or "full") and non-aromatic (empty) rings, determined by a simple, well-known, and widely-used aromaticity index, NICS(1)[16-17] which however is not free of drawbacks or discrepancies[17]. It is evident that in any polycyclic system (PAH, NGR, etc) not all the rings could be aromatic because the carbon atoms which "donate" the π-electrons belong to more than one (usually three) adjacent rings. The aromaticity pattern is pictorially described here by full red dots at the centers of the aromatic rings, which are also known as "full" rings. As is explained below, due to symmetry (and shell structure) there could be only two types of aromaticity patterns, for fully developed structures with well-defined symmetry.

2.2.3 The Shell Model and the "Main sequence of PAHs" The "main sequence of PAHs" consists of n layers (or geometrical shells),with a benzene

"nucleus" surrounded by n-1 annulenes rings (a total of n shells) one inside the other like a Russian babushka doll. These PAHs serve as a bridge from benzene and graphene, as more and more shells are added in the limit $n \to \infty$, where n is the "shell number". Although this sequence was invoked for describing the electronic (and aromatic) properties of Graphene[1], these PAHs and their geometrical/topological variations and interrelations are the subject and the focus of the present study. As is shown in Fig. 1(a), these PAHs (with possible exception of benzene and coronene) are zigzag bonded, although zigzag edges have been "demonized" as peculiar and non-aromatic. This is because isolated zigzag bonds, in contrast to armchair ones, violate the bipartite or "sublattice" symmetry and balance. Yet, by eliminating the empty edge rings ("inert rings) we can eliminate the zigzag edge and obtain the "homologous" PAHs with armchair bonds, and larger HOMO-LUMO gaps, as sown in the second row of Fig. 1(a). Likewise, topologically frustrated, and "elusive" structures, which are best candidates for non-conventional magnetism[8-11] are almost invariably zigzag terminated. This last category of structures, which violates the fundamental bonding rules of Kekulé[7-9] (and Clar's as well), corresponds in the present scheme (of aromaticity patterns) to frustrated or "irregular", and/or "faint" aromaticity patterns characterized by very low (or zero) NICS(1) value(s). As we can see below, these structures can also improve their stability and properties (sublattice imbalance) by such elimination process. The main sequence of PAHs has been expanded in the present study up to n=12. As we can see in Fig. 1(b), the HOMO and LUMO densities are more and more localized at the edges as the size increases, which is considered a natural consequence of the shell structure suggesting that electronic valence states should mainly concentrated at the geometrical valence shell. Besides the aromaticity patterns in Fig.

1(c) and 1(d), which will be discussed in section 2.2.2, we can observe in Fig. 1(e) the soft vibrational modes which tend to create a corrugated structure of D_{3d} symmetry.

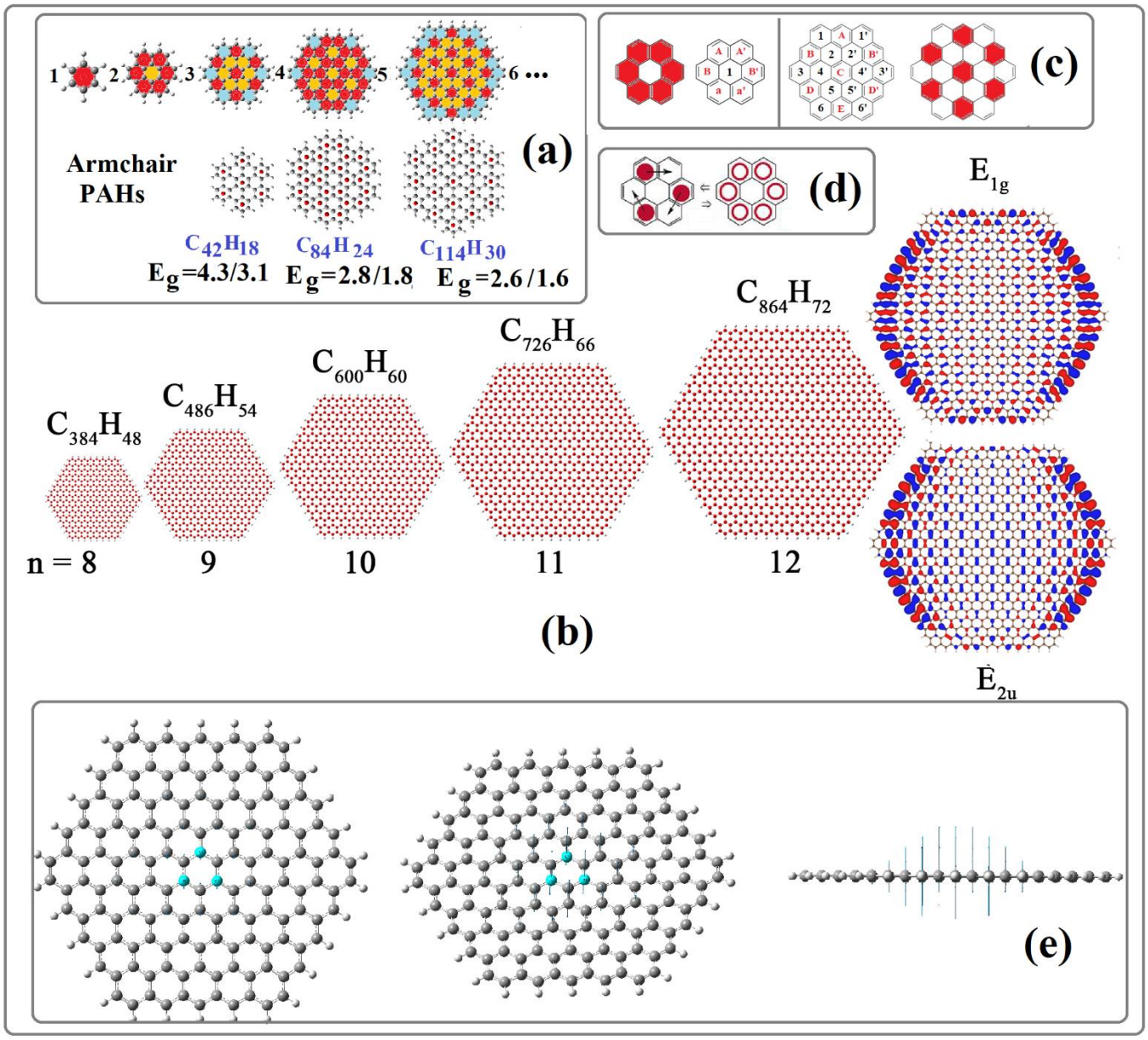

FIGURE 1. The first five members of the "main sequence" with their stoichiometry, aromaticity patterns, and "Hückel count", together with the resulting armchair PAHs in the second row **(a)**. The full, empty, and "inert" rings are highlighted with red, yellow, and light blue colour, respectively. Extension of the main sequence up to n=12. Representative HOMO and LUMO orbitals are shown for the n=12 PAH **(b).** Illustration of the two aroamaticity patterns **(c)** and the migration of sextets **(d)**. The

soft vibrational mode, and the corresponding displacement pattern (exaggerated for better visibility) of the n=5 PAH, shown from different angles of view is illustrated in **(e)**.

These modes are of B_{2g} and E_{2u} symmetries with the two sublattices vibrating against each other, and as is shown in Fig. 1(e), they are concentrated on the "soft core" of the shells, whereas the valence shells remain practically stationary. In the D_{3d} geometry the largest deviation from planarity is of the order of 0.001 Å, for the n=5 PAH shown in Fig. 1(e). In the corrugated D_{3d} geometry the softest (lowest frequency) mode corresponds to vibrations of the (geometrical) valence shells, whereas the soft core remains practically stationary. For the analogous hexagonal structure of silicene, the same modes correspond to purely imaginary frequencies. Distortion according to these imaginary frequency modes leads to a buckled D_{3d}-symmetric structure, where the maximum deviation from planarity is now of the order of 0.1 Å for the n=4 shell. It should be stressed at this point that in both cases the D_{3d} symmetry, contrary to D_{3h}, includes center of inversion (like D_{6h} PAHs and graphene itself) which preserves the symmetry competition (between molecular and sublattice symmetry groups). Such competition is responsible for the exotic properties of graphene. In contrast, heteroatomic "hexagonal" structures of real D_{3h} symmetry, as BN or SiC, have identical molecular and sublattice symmetry groups without inversion symmetry center. These structures, based only on symmetry, can be understood as not graphene-like.

2.2.4 The Aromaticity Patterns Using the shell model, we see that we could have two aromaticity patterns (compatible with D_{6h} symmetry); one in which the central benzene ring ("nucleus") is aromatic, as in benzene and circum-coronene (CIRCO); and one in which the central ring is non-aromatic (empty) and the first (hexagonal) shell is

aromatic, as in coronene (CO). This is illustrated in Fig. 1(c). Then, shell periodicity and the D_{6h} symmetry operations will generate the aromaticity patterns of the rest PAHs, consistent with the symmetry requirements, as in Fig.S1, and 1(a). It is clear that in order for the central ring to be aromatic, the shell number (which is equal to the total number of rings) should be odd, since due to (inversion) symmetry there should be an equal number of empty rings left and right of the central ring. On the other hand, if the central benzene ring is empty the inversion symmetry requirement is automatically satisfied. Thus, for odd shell numbers the central ring would be aromatic, and the aromaticity patterns would be of the CIRCO type consistent with Clar's rule(s)[18] of sextets (6μ), or in other (more technical) words there would only one unique Clar formula[18]. In addition, Hückel's rule of 4m+2 π-electrons would be satisfied as well, since there is an odd number of shells in each one of which Hückel's rule is satisfied.[1] Therefore we can state: 6μ=4m+2. Moreover, in this case the parity of the HOMOs would be even (e_{2g}), since there is an even number (l=n-1) of shells around the "nucleus".[1] The parity of the LUMOs, reflecting the HOMOs of the next shell would be odd (e_{1u}). On the contrary, for even shell numbers the aromaticity pattern would be of CO type violating both Clar's and Hückel's, since the sum of an even number of terms of the form 4m+2, would be of the form 4k. The remedy in this case is to ignore the intermediate and consider only the outer shell (in which Hückel's rule is satisfied by default). This we could call "generalized Hückel's rule". The corresponding remedy for Clar's rule is the "migration of sextets" which is a superposition of two equivalent Clar's formulas, as is shown in Fig. 1(d). In this case the CO type aromaticity can be considered as enhanced by the migration of sextets. We could jokingly call then the corresponding collective excitations (or aromaticity entities) "sextons". The Parities of the HOMOs and LUMOs have been reversed from the ones of odd shell numbers.

We should also observe that in both cases (odd or even shell number) the empty rings, contrary to full rings are compatible with the symmetry of the next shell structure, or the unoccupied LUMOs of the current structure. Therefore, within the current structure and symmetry, elimination of these empty rings would be expected to improve (increase) the HOMO-LUMO gap and the aromatic/electronic properties, without altering the aromaticity pattern. As we can see in Fig. 1(a), this is indeed the case.

2.2.5 Computational Methods. The theoretical and computational framework of this work, which includes a multitude of systematic and interconnected (one-body) DFT calculations on PAHs, NGRs and GNRs (AGNRs) of given symmetry, has been discussed in sections 2.2.2-2.24 and earlier.[1-2] In the present work the "main sequence" of hexagonal PAHs, which defines the shell structure, has been expanded and extended to include larger PAHs, and analogous rectangular NGRs and GNRs (AGNRs), analyzed in terms of simple group theory and topological concepts and connections. All geometrical structures have been optimized (or reoptimized) using tight convergence criteria at the DFT level of the hybrid PBE0[20] functional using the 6-31G(d) basis set, as is implemented in the GAUSSIAN program package (G09)[21]. Similarly, the CCSD and CCSD(T) calculations were performed with G09. The same package was also used for the calculation of NICS(1) aromaticity index, which for the present work has been proven satisfactory and suitable[1-4, 16-17]. This level of theory, used consistently and uniformly for all structures small and large (for all related properties), is fully adequate for such calculations, as was pointed out earlier.[1-4, 14] For the visualization of the results (orbitals, electronic and spin densities) the GaussView[22] program was used.

3. Results and Discussion.

3.1 Hexagonal PAHs. As we have seen in Fig. 1(a), the armchair PAHs which have been obtained by the elimination process, have the same aromaticity pattern (but larger HOMO-LUMO gaps). Moreover, these armchair PAHs have more in common with their zigzag parent structures beyond the aromaticity pattern. Such common properties include the structure and symmetry of the HOMO and LUMO orbitals, as is shown in Fig. S2 for HEXCO and CIRCO. These characteristics are invariant under the "truncation" transformation and are intimately connected with the shell number and the number of hydrogen atoms (although differently bonded), which are also invariant. Besides the obvious identity of the shell numbers (since the remaining peripheral rings belong to the same "valence" shell), the equality of the number of hydrogens follows, from the "effective shell number", which for hexagonal PAHs with incomplete shells (as HEXCO) is defined as the 1/6 of the number of hydrogens,[1] from the 6n hydrogens in the full-shell PAHs. of the main frequency. Thus, aromaticity patterns, shell number (effective or not) and symmetry of HOMO and LUMO orbitals, which are all interconnected remain invariant under truncation. Yet, although the aromaticity patterns are the "same" (the same rings are "full" before and after the "truncation"), the ring currents and the NICS(1) values could be lower, as is illustrated in Fig. S3 for the n=3 PAHs (CIRCO and HEXCO). The average NICS(1) value drops from -17.6 ppm in CIRCO to -12.1 ppm in HEXCO. This should be expected within the shell model[1] since the truncation process renders the valence shell incomplete, but in a symmetrical way (i.e. keeping the hexagonal symmetry). For the corresponding electrons, this means that the 12 π-electrons removed, corresponding to the 12 carbon atoms eliminated, were distributed equally between MOs of positive and negative parity, as well as between nondegenerate and degenerate MOs, corresponding to 1-dimensional (1D), and 2-dimensional (2D) irreducible representations (2D) respectively, of the molecular

symmetry group. Indeed, the missing electrons can be verified to have been taken out of the following configuration(s): $(b_{1g})^2(e_{1g})^4(a_{2u})^2(e_{2u})^4$, which fulfil the above conditions. Note that both CIRCO and HEXCO are stable and abundant, which is highly suggestive that such truncation transformation constitutes a natural process. In section 1.3 in SI, the balanced electronic configurations of the removed rings are also illustrated for the n=4, and n=5 PAHs. For example, the 36 removed electrons for n=5 belong to the configuration(s): $(b_{1g})^2(b_{2g})^2(e_{1g})^4(e_{2u})^4(e_{1g})^4(e_{2u})^4(a_{2u})^2(a_{1u})^2(e_{1g})^4(b_{1g})^2(e_{2u})^4(a_{2u})^2$, which are perfectly balanced (three odd 1D and 2D, and three even 1D and 2D representations). This guarantees the perfect similarity with the parent structure, which also includes bond-length distributions (see Fig. S4). Furthermore, in Fig. S5, is illustrated that the truncation process can be performed in more than one steps, provided each empty- peripheral-ring elimination preserves the hexagonal symmetry. Obviously, in this case, the intermediate structures are not expected to have the same degree of "perfection" as the final. For the n=6 PAH, the results shown for the n=6 PAH in Fig. S6, also emphasize the excellent HOMO, LUMO matching of the initial zigzag PAH $C_{216}H_{36}$ and the transformed armchair "homologous" hexagonal PAH $C_{180}H_{36}$. Finally, it is important to emphasize that the truncation process introduced here is a much more general process, well beyond the PAHs of the main sequence (and the hexagonal symmetry). In Fig. 2, especially in Fig. 2(b), this process is applied for the hexagonal PAHs (with more than one geometrical open shells) $C_{252}H_{48}$ with a gap of 1.7 eV, which is gradually transformed by this process to the geometrically closed shell $C_{180}H_{36}$ PAH of the main sequence with n=6 (shown in Figs. 2(a) and S6) with a HOMO-LUMO gap of 2.1 eV. It is interesting to observe in this case, that the final structure does not have the same number of hydrogens (or effective shell number), but preserves the same aromaticity pattern, since the effective shell number changes by 2 units, keeping the

same parity (even). Figure 2 also illustrates a different way of truncation in which only alternant groups of empty peripheral rings are eliminated. The resulting structures have triagonal (D_{3h}) symmetry, subgroup of D_{6h}, and are discussed in the next section.

3.2 Triagonal PAHs and NGRs

3.2.1 Armchair NGRs

The n=6 PAH in Fig. 2(a), shown also in Fig. S6, can be also transformed in an alternative ("alternating") way, as is shown in the upper part of Fig. 2 (a). Following the route (1) to (3), in the second row, instead of (1) to (2) in the first (top) row, we can delete every other group of empty rings, resulting in the triangular structure $C_{198}H_{36}$. This structure (3), $C_{198}H_{36}$, with (mainly) armchair bonds, following the same method of elimination, results in the all-armchair bonded structure (4), $C_{162}H_{36}$, with no empty peripheral rings (and, thus, "aromatically irreducible"). We can also observe that, although the parent hexagonal structure is characterized by a "Hückel count" of 4k and a "compatible" hexagonal CO aromaticity pattern, both triangular structures (3) and (4) have opposite "Hückel count" (4k+2), and "opposite" CIRCO aromaticity pattern. However, as we can verify in Fig. 2(b), and below in Fig. 3(a), the "Hückel count" is irrelevant for the outcome of such truncation process, but the triagonal CIRCO pattern and the armchair bonds are general and invariant characteristics for all of them.

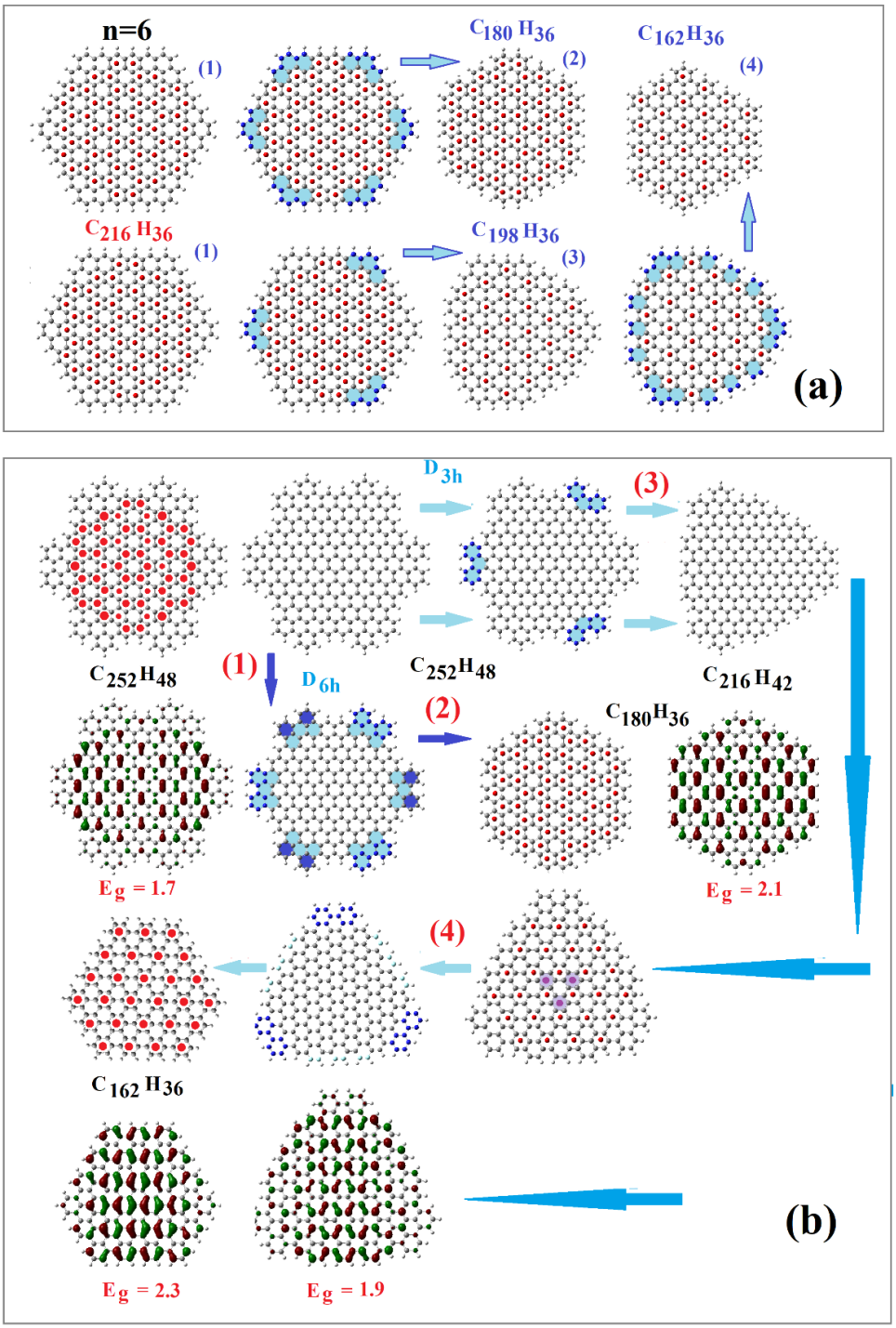

FIGURE 2. **(a)** The routes for the "closed shell" hexagonal (D_{6h}) zigzag PAH with n=6 to the "homologous" armchair PAH (with n_{eff} =6), (1)-(2), and to "daughter" D_{3h} PAHs, (1)-(3)-(4). Empty peripheral rings are highlighted with light blue color (on line). **(b)** Similar routes for the "open shell" n_{eff} = 8 PAH, including also initial, intermediate, and final HOMO

orbitals and HOMO-LUMO gaps (E_g). Dark blue highlighting emphasizes D_{6h} versus D_{3h} eliminations, whereas purple highlighting indicates "anomalous" rings (see text).

This can be understood from the fact that in this case the molecular and the (sub)lattice symmetry groups are the same (D_{3h}) with no inversion symmetry, and therefore no symmetry conflict (which was the underlying reason for the frustration and the "generation" of the CO pattern) and the Dirac points[2-4]. For the same reason both HOMO and LUMO orbitals have the same (e") symmetry, as can be seen at the bottom part of Fig. 2(b) and Fig. 3(a) below. The intermediate triagonal structure (4) with stoichiometry $C_{216}H_{42}$ (which also has a "Hückel count" of 4k, not 4k+2 as the other triagonal structures in Fig. 2) is characterized by an anomalous triagonal aromaticity region (shaded in the figure, apparently related with the remaining zigzag bonds), which disappears after final ring removal (step 4 in Fig. 2b). Furthermore, we can see (in Fig.2a) that the number of Hydrogen atoms at the edges during the $D_{6h} \rightarrow D_{3h}$ transformation remains the same. However, as we can also verify in Fig. 2(b), this is true for closed shell (geometrically/topologically) D_{6h} PAHs[1] or other "aromatically irreducible" e.g., all-armchair D_{6h} structures. As was mentioned earlier for the geometrically/topologically open-shell PAHs, as $C_{252}H_{48}$, this is not true (neither for the intermediate D_{3h} structure (4), which is not all chair-bond bonded and "reducible aromatically"). In contrast, the (aromatically irreducible) $C_{162}H_{36}$ D_{3h} PAH, preserves the number of hydrogens (and therefor the "shell number") with the ("aromatically irreducible") $C_{180}H_{36}$ D_{6h} structure. Most of the conclusions drawn from Fig. 2, are verified and "fortified" in Fig.3. Figure 3(a), which is the triangular analogue of Figs. 1(a) and S1, shows the analogous triangular "main sequence"[1] as the corresponding "shell index" runs up to 6. As we can verify, all triangular PAHs of the main sequence are armchair bonded at their edges, have no empty peripheral rings (therefore they can be characterized as "aromatically irreducible")

and have exactly the same CIRCO aromaticity pattern, irrespectively of the number of π-electrons (number of carbon atoms) and (apparently) of the "Hückel count". Furthermore, there is no alteration in the symmetry of the HOMO, LUMO orbitals of a given PAH, neither between the HOMO's of successive PAHs, as in Fig. S1, due to the absence of inversion symmetry. Thus, both HOMO and LUMO are topologically identical, having the same e'' symmetry. As was explained above, this is a consequence of the coincidence of the molecular and (sub)group symmetries. As a result[2-3], there should be no Dirac points in such PAHs, and their properties would be expected to be different from those well-known properties of graphene-like PAHs (and graphene itself), especially those directly related with Dirac's points. Therefore, no edge states should be present inside the gap.[3-4] This is partially reflected in the variation of HOMO-LUMO gap in Fig. 3(b), which shows much larger gaps (for a given shell number) from both zigzag and armchair hexagonal PAHs. This should be related to their "correct" aromaticity pattern, and to some extend to quantum confinement due to the smaller size of triangular NGRs for a given shell number (although the number of electrons could be smaller as well). Thus, although triagonal armchair nanographenes could be very efficient for appreciable bandgap opening (especially in view of the absence of topological edge states around the Fermi level), they would not be expected to have the exotic properties of graphene and other NGRs, which are related with Dirac's points. Finally, we can observe in Fig. 3(b) that hexagonal armchair PAHs, contrary to the other two categories (Hexagonal zigzag and triagonal armchair) which show a smooth variation of the HOMO-LUMO gap in terms of the shell number, show clearly higher gaps for odd shell numbers, i.e. for PAHs satisfying both Clar's rule(s0 of sextets and Hückel's rule of 4n+2 π-electrons, compared to those of even shell number, suggesting higher aromaticity for the odd-shell-number PAHs.

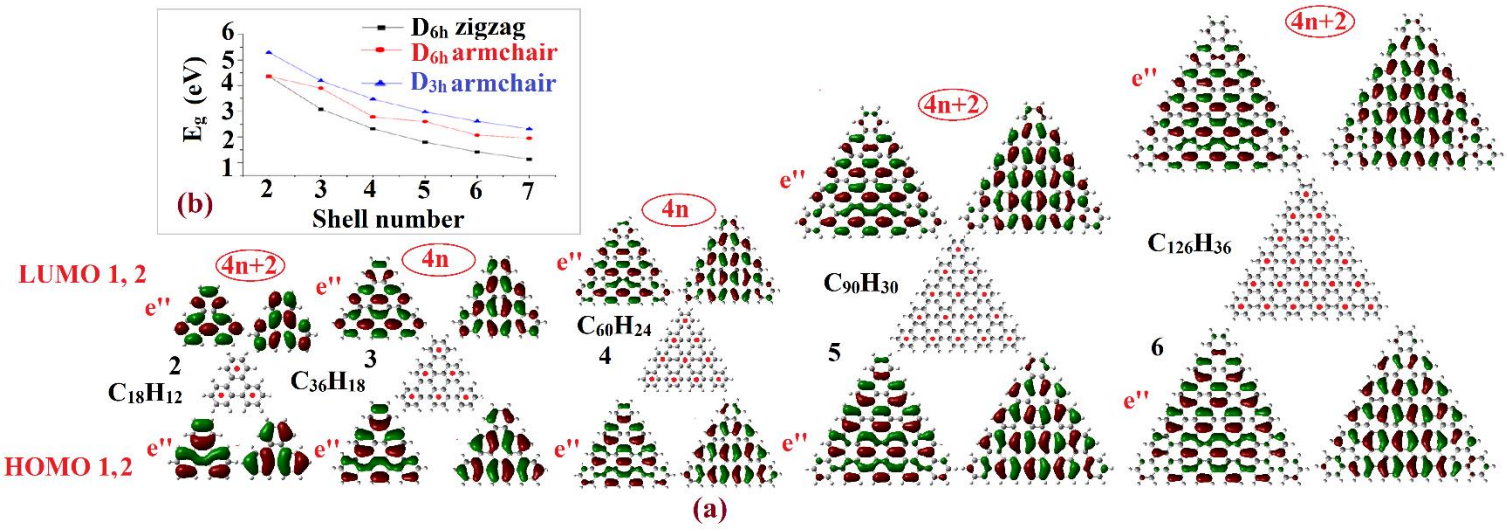

FIGURE 3. (a): A triangular version of the main sequence of PAHs[1], their aromaticity patterns, and their doubly degenerate e'' HOMO (1,2), LUMO (1,2) frontier orbitals in analogy to the hexagonal main sequence, for n=2-6; including, stoichiometry, "Hückel count" (4n, 4n+2), and "shell number" (see text). **(b)**: HOMO-LUMO gap (E_g) variation in terms of "shell number" for: hexagonal zigzag (black), hexagonal armchair (red), and triagonal armchair (bleu) PAHs.

3.2.2 Zigzag NGRs Contrary to armchair triagonal NGRs, zigzag triangular NGRs, not only are not aromatic, but they are topologically frustrated unstable and highly reactive open shell states, with (high) spin, depending on their size, due to inherent sublattice imbalance leading to unpaired electrons. In the aromaticity pattern picture adopted here, as we can see in Fig.4, this corresponds to very low aromaticity indices, such as NICS(1). Such structures clearly violate both Hückel's and Clar's rules, as is illustrated in Fig. 4 (*e.g.* by adjacent "full" rings). As a result, the NICS(1) values obtained (and displayed in Fig. 4) are very small with an average value around -6 ppm (compared to about -11.5 ppm for benzene), with the largest absolute value (-7 ppm) for the 2-triangulene ($C_{13}H_9$) in Fig. 4(a), which is actually a borderline case with practically armchair bonds. Despite their topological frustration and high

reactivity these triangulenes have been recently synthesized by novel techniques. The 3-triangulene was “synthesized” by manipulating physically atoms on individual molecules using the tip of a scanning tunnelling microscope (STM)[5]. The extended 4- and 5- triangulenes were synthesized by precise bottom-up synthesis using suitable molecular precursors on metallic surfaces.[6-7] Looking at Fig.4, we can observe in the right portion of Figs. 4(b) and 4(c) that in both (and all) these cases the truncation process of eliminating “empty” peripheral rings, leads to better (larger absolutely) values of the average NICS(1) values, and lower spin values (by tree spin units), which are connected with the lattice imbalance N_A-N_B. Thus, the resulting structures have reduced (or none) lattice imbalance and smaller degree of topological frustration, and consequently better stability. For example, it is important to observe that, although the 4-triangulene is characterized by N_A=25, N_B=21, and N_A-N_B=4, with spin 4/2=2, the aromatically reduced structure $C_{24}H_{18}$ on the right portion of Fig. 4(b) is characterized by N_A=12, N_B=12, and N_A-N_B=0, with spin 0, without topological frustration, a large 5.1 eV HOMO-LUMO gap, and a large absolute value of average NICS(1) equal to -9.85 ppm (-8.2 ppm for the central ring and -10.4 ppm for each peripheral ring) close to the value for benzene. Moreover, the planar D_{3h} $C_{24}H_{18}$ structure is found not to be the global (or local) minimum of the energy hypersurface since it is characterized by a doubly degenerate e’’ mode of imaginary frequency. However, when the planar structure is distorted according to the imaginary frequency mode, turns into a very well-known stable and naturally abundant structure of C_2 symmetry (in which the peripheral benzene rings are not in the same plane as the central ring). This is 1, 3, 5-Triphenylbenzene, with an extra stability of 0.33 eV in total energy, and a calculated HOMO-LUMO gap of 5.5 eV, which a very stable, and abundant molecule well-known both in the molecular and crystalline phase.[23] This illustrates the (unexpected) efficiency and consistency of this process, on top of its transparency and simplicity.

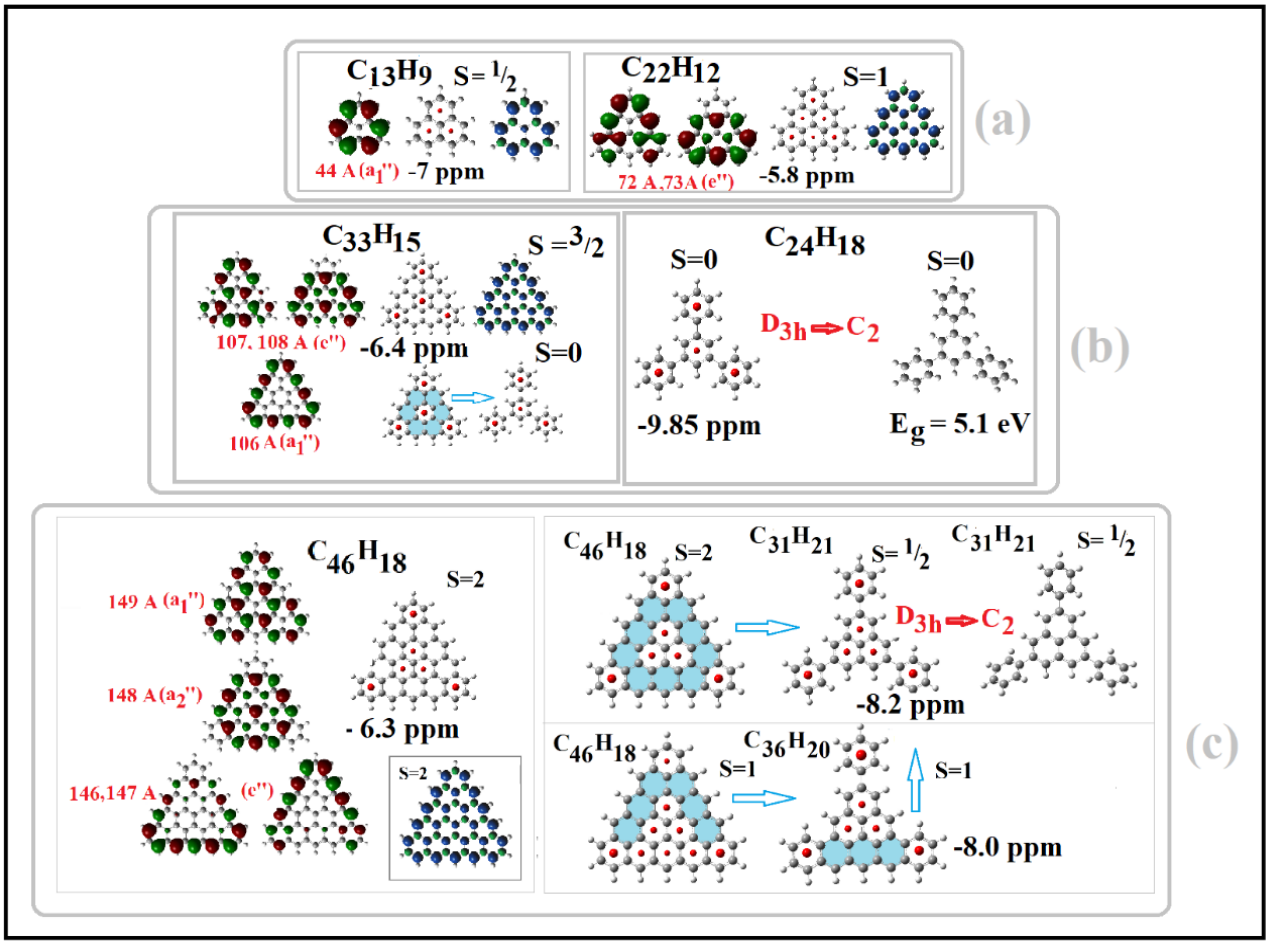

FIGURE 4. Electronic, Aromatic, and topological properties of the 2-, 3-triangulenes $C_{13}H_9$, $C_{22}H_{12}$ (a); 4-triagelene $C_{33}H_{15}$ (b), and 5-triangulene, $C_{46}H_{18}$ (c); including SOMOs (isovalue =0.2), with spin and space symmetry and orbital number; aromaticity patterns, and spin density (isovalue=0.004). Aromaticity patterns, based on the NICS(1) number (the average value of which, <NICS(1)>, is shown in ppm), are described by indicating the "full" (or not entirely empty) rings with red dots on their centers. For the 4- and 5- triangulenes the truncation process of the "empty" peripheral rings (highlighted by light blue colour on line) is also described in the right portion of Figs. 4(b), and 4(c), respectively (see text).

Moreover, in view also of the example of the aromatic pairs of circumcoronene and hexabenzocoronene, seen earlier, one could suggest that the "truncation process" uncovered

here could be not just a conceptual and efficient physicochemical tool, but a natural process as well. Such possibility is very intriguing, rendering special significance and importance in the present results. A similar process for the 5-triangulene ($C_{46}H_{18}$), as is illustrating in the right part of Fig. 4(c), leads first to the D_{3h} planar $C_{31}H_{21}$, with lattice imbalance N_A-N_B=1 and spin ½ (lower by 3 units, as before), and finally to the C2-symetric isomer which could be characterized as the three-phenyl substituted 2-triangulene (in Fig. 4(a), left portion). In the bottom line in the right part of Fig. 4(c), we can see a different form and version of the partial elimination (illustrated in Fig.2). If we choose the parent (5-trangelene) structure with the wrong spin, 1 instead of the correct 2, the geometry optimization leads to a planar C_{2v}-symmetric structure with full and empty rings as shown in the Figure (bottom right of Fig. 4(c)) $C_{36}H_{20}$, which following the next elimination process, leads again to the three-phenyl-substituted 2-triangulene ($C_{31}H_{21}$), as it should. This verifies emphatically the strong interrelation between topological (geometrical) and electronic characteristics, (electron spin in particular) for the triangulenes. This is in contrast to AGNR's zigzag ends,[3-4] where the triplet-singlet energetical ordering is reversed when correlation is included, indicating that possible observed magnetism should be no conventional in the sense that it should not be directly related with spin, but rather with pseudospin (i.e. rearrangement of p_z orbitals). [3-4] In triangulenes, as we can see in table 1, the triplet state is lower energetically before and after correlation (at the level of coupled clusters CCSD, with and without inclusion of perturbative triplet contributions (T), using the 6-31g(d) basis set), the inherent sublattice imbalance leads to open states with real spin and not pseudospin. This can be further illustrated for the 3-triangulene ($C_{22}H_{12}$), which with an even number of electrons (and atoms), is predicted (and verified) be open shell with spin equal to 1. This is consistent with the lattice imbalance N_A=10, N_B=12 ($|N_A-N_B|= \eta= 2$, $S=\eta/2=1$). The nullity η gives

the number of zero eigenvalues in the TB Hamiltonian, which in turn is equal to the number of singly occupied molecular orbitals (SOMOs).

TABLE 1. 3-Triangulene. Comparison of the Total energies of singlet and triplet states.

Method	**Singlet Energy (hy)**	**Triplet Energy (hy)**	**Triplet-Singlet (eV)**
DFT/PBE0	-844.5901863	-844.632982	-1.164
HF	-840.0612321	-840.228858	-4.559
CCSD	-842.914112	-842.968228	-1.472
CCSD(T)	-843.0791947	-843.1054334	-0.714

The SOMOs for this and the other triangulenes are shown in Fig.4 (a, b, c), whereas the complete energetical structure of the orbitals around the Fermi level is shown in Fig. S8. As we can see in Fig. 4(a) the two SOMOs for this triangulene are not localized at the edges (apparently due to quantum confinement), neither the spin density, as is several times mentioned in the literature. However, looking at the higher (4-, 5-) triangulenes in Fig. 4(b, c), we can see that some (almost half) of the SOMOs are indeed localized at the edges. In the same figure we can also see that the larger values of spin density are located at the edges, on C atoms of one (the "majority") sublattice. Nevertheless, smaller values are also found in the interior where several SOMOs are (de)localized, forming the sublattice pattern (structure). This should be expected since the spin values are directly related with the sublattice imbalance. Similar results for the 6-triangulene are summarized in Fig. S9, following the same rules, guidelines, notation, and conclusions.

4. AGNRs. In ref. 3 it was illustrated that zigzag end states, localized at the zigzag ends of relatively thin and finite AGNRs can be generated due to the symmetry conflict

between sublattice and molecular symmetry groups. The resulting geometrical /topological frustration is maximized at the central region (middle) of the AGNR, thus pushing the electronic density of the frontier orbitals to the two ends.[3] Recently[4], it was realized that due to quantum confinement, there is a lower critical length limit needed for such end states to develop. Thus, no end states can be observed for AGNRs of length smaller than the critical length, which for the very narrow 5-AGNRs is found to be about 10 nm.[4] Figure 5 shows the example of the 4x24 or (9, 48) AGNR of width 9 and length 48 carbon atoms, with the end states at the two ends and the aromaticity pattern found with the NICS(1) aromaticity index. Following the elimination technique of the inert rings that we have discussed and applied above, we are led to the edge-modified 9-AGNR in the right part of the figure. As we can clearly see the end states (and the zigzag ends) have been eliminated, as was expected. At the same time the HOMO-LUMO gap of the edge modified 9-AGNR was increased by more than 1 eV. This is a very useful, representative example of gap opening.

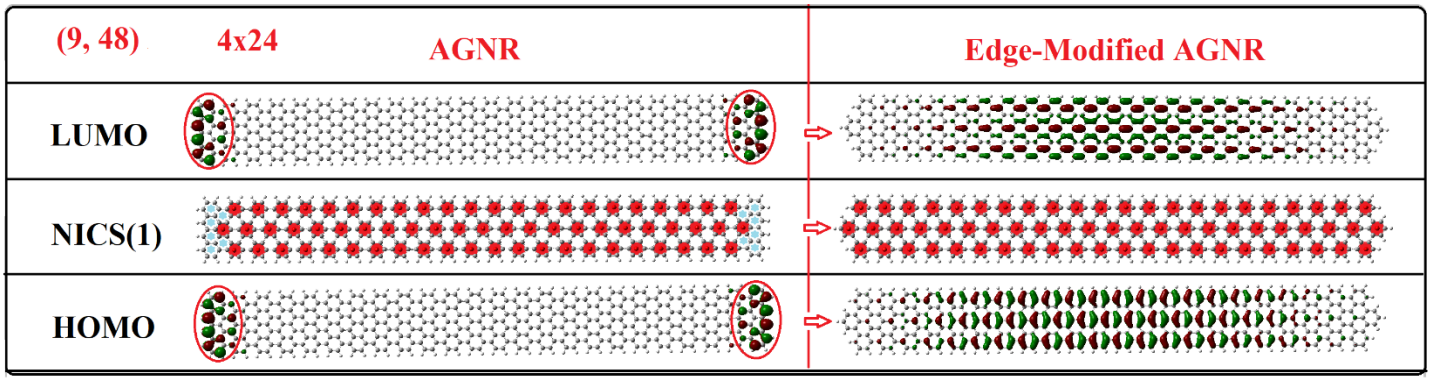

FIGURE 5. 4x24 or (9,28) AGNR. Left: Elimination of end-states, marked with red ellipses, by eliminating the "inert" rings, marked with small light blue stars. Right: Resulting AGNR without zigzag ends, and end states.

5. Conclusions. By using and enriching the shell model[1] and related simple aromaticity concepts it has been shown that:

1) Hückel's and Clar's rules of aromaticity are intimately interrelated and for hexagonal NGRs and PAHs with odd "shell number" they are equivalent, satisfied simultaneously; whereas for "even shell number" they both fail (without additional external assumptions such as the generalized Hückel's rule, and the migration of sextets).

2) We can functionalize the electronic and aromatic properties of PAHs and NGRs and increase the HOMO-LUMO gaps (bandgaps) by controlling the empty peripheral rings, which are intimately connected with the zigzag bonds, without altering the form and symmetry of the frontier orbitals and the corresponding aromaticity patterns.

3) Elimination of "inert" rings from the zigzag ends of AGNRs leads to AGNRs without topological end states and "magnetism" and with significantly larger HOMO-LUMO gaps.

4) By eliminating empty (non-aromatic) peripheral rings in hexagonal zigzag NGRs we get armchair NGRs with improved properties (larger band gaps)

5) Partial elimination under D_{3h} subgroup leads to triangular armchair NGRs with armchair bonds with one unique Clar-type aromaticity pattern, independently of shell-number, parity, and number of π- electrons.

6) Triangular nanographenes are shown not to be graphene-like, in the sense that they have no Dirac points, which are generated by the competition between molecular and sublattice symmetry, due to identical molecular and sublattice symmetries (D_{3h}). Thus, triagonal nanographens should be either fully (Clar) and uniquely aromatic with armchair-edges, or non-aromatic and "frustrated", with zigzag-edges and high (true) spin.

7) Applying the same strategy of truncation (elimination of empty peripheral rings) to zigzag triangular NGRs (triangulenes) we get more stable structures with smaller sublattice imbalance and spin, by 3 units. In the case of the extended [4]-triangulene, we finally obtain the 1,3,5-triphenylbenzene which is a stable naturally abundant molecule with closed shell structure (S=0), large (5.5 eV) HOMO-LUMO gap, and NICS(1) value close to benzene.

8) Based on paradigms of hexabenzocoronene and triphenylbenzene, it is suggested that this could be a natural (not just a conceptual or mechanical) process.

9) Finally, it is suggested that this process should be very useful for other graphene nanostructures for the manipulation (perhaps by STM tip methods) and functionalization of their structural, electronic, aromatic, and magnetic characteristics simultaneously.

Thus, further work on this subject (both experimental and theoretical) should be important.

References

1. Zdetsis, A. D. Classics Illustrated: Clar's Sextet and Hückel's (4n+2) π Electron Rules. *J. Phys. Chem. C*, **2018**, 122, 17526-17536.
2. Zdetsis, A. D. Bridging the Physics and Chemistry of Graphene(s): From Hückel's Aromaticity to Dirac's Cones and Topological Insulators. *J. Phys. Chem. A* **2020**, 124, 976-986
3. Zdetsis, A. D. Do We Really Understand Graphene Nanoribbons? A New Understanding of the 3n, 3n±1 Rule, Edge "Magnetism" and Much More. *J. Phys. Chem. C* **2020**, 124, 7578−7584

4. Zdetsis A. D.; Economou, E. N. Topological Metal-Insulator Transition in Narrow Graphene Nanoribbons?, *Carbon* **2021** 176, 548-557
5. Pavliček, N. *et al.* Synthesis and characterization of triangulene**.** *Nature Nanotechnol.* **2017,** 12, 308–311 DOI:10.1038/nnano.2016.305
6. Mishra, S. ; Beyer, D.; Eimre, K. *et al.* et al. Synthesis and characterization of π-extended triangulene. *J. Am. Chem. Soc.* **2019** 141, 10621–10625
7. Su, J.; Telynchko, M.; Hu, P. et al. Atomically precise bottom-up synthesis of π-extended [5] triangulene. *Sci. Adv.* **2019** 5, eaav7717
8. Mishra, S.; Beyer, D.; Eimre, K. *et al.* Topological frustration induces unconventional magnetism in a nanographene. *Nat. Nanotechnol.* **2020,** 15, 22–28
9. Wang, W. L., Yazyev, O. V., Meng, S. & Kaxiras, E. Topological frustration in graphene nanoflakes: magnetic order and spin logic devices. *Phys. Rev. Lett.* **2009** 102, 157201
10. Yazyev, O. V. Emergence of magnetism in graphene materials and nanostructures. *Rep. Prog. Phys.* **2010**, 73, 0565
11. Tucek, J.; Btonski, P.; Ugolotti, J.; Swain, A. K.; Enoki, T.; Zboril, R. Emerging chemical strategies for imprinting magnetism in graphene and related 2D materials for spintronic and biomedical applications. *Chem. Soc. Rev.* **2018**, DOI: 10.1039/c7cs00288b
12. Hofman R. The Many Guises of Aromaticity. *Am. Sci.* **2015**, 103, 18
13. Boldyrev, A. I.; Wang L.-S. Should Aromaticity Be Reserved For Only Benzene And Its Derivatives? Chem. & Eng. News online 2015, http://cenm.ag/aromatic
14. Sola, M. Why Aromaticity is a Suspicious Concept? Why? *Front. Chem.,* **2017**, 5, 22 .
15. Zdetsis, A. D.; and Economou, E.N. Electronic and aromatic properties of graphene and nanographenes of various kinds: insights and results, *Adv. Mat. Lett.* **2017**, 8, 256-261

16. Schleyer, P.v.R.; Maerker, C.; Dransfeld, A.; Jiao, H.; van Eikema Hommes, N.J.R. Nucleus Independent Chemical Shifts: A simple and Efficient Aromaticity Probe, *J. Am. Chem. Soc*. **1996**, 118, 6317–631
17. Sola, M.; Feixas, F.; Jimenez-Halla, J. O. C.; Matito, E; Poater, J. A Critical Assessment of the Performance of Magnetic and Electronic Indices of Aromaticity. *Symmetry*, **2010**, 2, 1156-1179
18. Clar, E. The Aromatic Sextet; Wiley: New York, NY, **1972**
19. Popov, I. A.; Bozhenko, K. V. ; and Boldyrev, A. I. Is Graphene Aromatic? *Nano Res.***2012**, 5, 117–123
20. Adamo, C.; Barone,V. Toward Reliable Density Functional Methods Without Adjustable Parameters: The PBE0 model. *J. Chem. Phys.*, **1999,** 110 6158-69
21. Frisch, M. J.; Trucks, G.W.; Schlegel, H. B.; Scuseria, G. E.; *et al*., Gaussian 09, Revision C.01, Gaussian, Inc., Wallingford CT, **2009**.
22. GaussView, Version 5.09, Dennington, R; Keith, T; Millam, J. Semichem Inc., Shawnee Mission, KS, 2016.
23. Prasad, D.; Preetam, A.; Nath, M. Experimental Crystal Structure Determination. *CCDC* 867818. **2013** DOI: 10.5517/ccy4147